Construction and Building Materials 107 (2016) 125–137

Contents lists available at ScienceDirect

Construction and Building Materials

journal homepage: www.elsevier.com/locate/conbuildmat

Comparison of different approaches for self-healing concrete in a large-scale lab test

Kim Van Tittelboom [a], Jianyun Wang [a,b,f], Maria Araújo [a,c,f], Didier Snoeck [a], Elke Gruyaert [a], Brenda Debbaut [a], Hannelore Derluyn [d], Veerle Cnudde [d], Eleni Tsangouri [e,f], Danny Van Hemelrijck [e], Nele De Belie [a,*]

[a] Magnel Laboratory for Concrete Research, Department of Structural Engineering, Faculty of Structural Engineering and Architecture, Ghent University, Technologiepark Zwijnaarde 904, B-9052 Ghent, Belgium
[b] Laboratory of Microbial Ecology and Technology, Department of Biochemical and Microbial Technology, Faculty of Bioscience Engineering, Ghent University, Coupure Links 653, B-9000 Ghent, Belgium
[c] Polymer Chemistry and Biomaterials Group, Department of Organic and Macromolecular Chemistry, Faculty of Sciences, Ghent University, Campus Sterre Building S4, Krijgslaan 281, B-9000 Ghent, Belgium
[d] Centre for X-ray Tomography/PProGRess, Department Geology and Soil Science, Faculty of Sciences, Krijgslaan 281, S8, B-9000 Ghent, Belgium
[e] Department of Mechanics of Materials and Constructions, Faculty of Engineering Sciences, Vrije Universiteit Brussel, Pleinlaan 2, B-1050 Brussels, Belgium
[f] SIM vzw, Technologiepark Zwijnaarde 935, B-9052 Ghent, Belgium

HIGHLIGHTS

- Both approaches have potential to be applied in real-scale concrete structures.
- Use of encapsulated PU requires more preparation compared to the addition of SAPs.
- One approach is triggered through crack appearance the other by water ingress.
- SAPs resulted in the highest healing efficiency based on crack width measurements.
- Release of PU from the capsules and crack closure was clearly noticed from CT.

ARTICLE INFO

Article history:
Received 21 August 2015
Received in revised form 17 December 2015
Accepted 24 December 2015
Available online 11 January 2016

Keywords:
Self-healing concrete
Superabsorbent polymers
Encapsulated polyurethane
Large-scale testing
Digital image correlation
Acoustic emission analysis
X-ray tomography

ABSTRACT

After several years of research in the Magnel Laboratory for Concrete Research (Belgium) to obtain concrete with self-healing properties, two of the most promising mechanisms were tested on a larger scale. One mechanism is based upon the encapsulation of polyurethane which is embedded in the matrix. Self-repair is obtained when crack creation causes capsule breakage, release and subsequent hardening of the polyurethane inside the crack. The second approach relies upon the addition of superabsorbent polymers (SAPs) to the concrete. These SAPs take up water entering via the crack, swell and block the crack. In addition, when they release their water content later on, they induce continued hydration and calcium carbonate precipitation. Real-scale concrete beams (150 mm × 250 mm × 3000 mm), with and without self-healing properties, were made and the self-healing efficiency was evaluated after crack creation by means of four-point bending. Based on the measured crack width reduction over time, it was shown that improved autogenous crack healing was obtained when superabsorbent polymers were added to the mixture. From the acoustic emission analysis, the proof of glass capsule breakage upon crack formation was obtained. X-ray tomography, fluorescent light microscopy and thin section analysis demonstrated that cracks were indeed partially filled with hydration products, calcium carbonate crystals and/or polyurethane which leached from the broken embedded capsules. Although it would be expected from both findings that this would result in a decrease of water ingress into the healed cracks, this could not be proven within this study.

* Corresponding author.
E-mail address: nele.debelie@ugent.be (N. De Belie).

http://dx.doi.org/10.1016/j.conbuildmat.2015.12.186
0950-0618/

1. Introduction

As concrete is a frequently used construction material but as it is susceptible to crack formation, which reduces the durability and increases the maintenance costs, self-repair of cracks in concrete is nowadays a very popular research topic. It was actually in 2001, when White et al. [1] published their paper in Nature about self-healing in polymer-based materials, that research on the development of self-healing materials gained a real boost and that attempts were taken to implement self-healing properties inside cementitious materials. In fact, concrete also possesses a kind of natural ability to repair damage to a certain extent [2]. If water enters into a crack and gets into contact with unhydrated cement particles, these can further hydrate resulting in crack closure. If both water and carbon dioxide enter, crack closure can be obtained through the precipitation of calcium carbonate particles from leaching calcium hydroxide. However, as the natural, named autogenous, crack healing mechanism is limited to small cracks [3], many attempts have been made to engineer concrete in order to obtain an improved, autonomous, crack healing efficiency.

Some approaches rather promote the autogenous crack healing ability by limiting the crack width through the addition of synthetic fibers [4] or by the use of shape memory alloys [5] which return to their original shape, and thus result in crack closure, upon heating. Other approaches promote the autogenous sealing and/or healing ability by providing an extra amount of water through the use of superabsorbent polymers (SAPs) [6–9]. SAPs take up water entering the cracks, swell and block the cracks against ingress of aggressive liquids. During dry periods, SAPs slowly release the absorbed water and provide it for further hydration and calcite precipitation. In other approaches, calcite precipitation is intensified by the addition of calcium carbonate precipitating microorganisms to the matrix [10,11]. Upon water ingress via the cracks these organisms start to consume available nutrients and precipitate calcium carbonate to close the crack. Next to these self-healing approaches, capsule-based [12,13] and vascular-based [14,15] mechanisms are reported, in which autonomous crack repair is obtained by release of a, mostly polymer-based, healing agent from embedded capsules or from a vascular system. Release of the agent is triggered through breakage of the capsules or the vascular system at the moment of crack formation.

We, in the Magnel Laboratory for Concrete Research (Belgium), started our research on self-healing cementitious materials in 2008. A number of the above-mentioned self-healing approaches have been investigated on lab-scale, resulting in diverse self-healing efficiencies. For this study, two of the most promising approaches were selected to be applied and tested on their efficiency on a larger scale.

2. Materials

2.1. Concrete beams with(-out) self-healing properties

The efficiency of two different self-healing approaches was compared in this study; self-healing by encapsulated polyurethane and self-healing through inclusion of superabsorbent polymers (SAPs). To prepare the beam where self-healing was obtained by release of polyurethane from embedded capsules (Table 1, PU), glass capsules were filled with the selected healing agent. About 350 glass capsules with a length of 50 mm and an inner and outer diameter of 3 mm and 3.35 mm, respectively, were first sealed with methyl methacrylate (MMA) at one end. Subsequently, the healing agent was injected into the tubular capsules by means of a syringe with a needle. In this study, a one component polyurethane-based healing agent, which was developed within the framework of this study, was applied. This agent hardens upon contact with humidity inside the concrete matrix. After filling of the capsules with healing agent, the other end was sealed with MMA glue. To position the capsules within the mould of the beam, a network of plastic wires was connected with the walls of the mould at a depth of 10 mm. Every 40 mm over the complete length of the mould, except the outer 160 mm, a wire connected one side of the mould with the other (Fig. 1A). Glass tubes were glued onto this network of wires by means of MMA glue. Each time five capsules were placed with an intermediate distance of 46 mm and at both capsule ends there was 5 mm overlap with the wires. The next row was then arranged in an alternating way compared to the previous row (Fig. 1B). Next to the network of capsules, this mould contained four reinforcement steel bars with a diameter of 10 mm. These were positioned underneath the network of capsules in order to obtain a concrete cover on top of the bars of 20 mm. In this way the network of encapsulated healing agent was positioned in the middle of the concrete cover layer and ingress of aggressive substances towards the reinforcement via cracks within the concrete cover could be avoided when the self-healing mechanism is properly activated due to crack formation.

For the second self-healing approach under investigation, being the use of SAPs to cause crack sealing and promote autogenous crack healing (Table 1, SAP), no additional preparation was needed compared to the reference beam (Table 1, REF), as the SAPs are added dry to the concrete upon mixing. The SAPs used within this study were cross-linked copolymers of acrylamide and acrylate which were obtained through bulk polymerization and have particle sizes below 600 μm. The SAPs have an absorption capacity of 308.2 ± 4.7 g/g SAP in de-ionized water and 37.9 ± 1.6 g/g SAP in cement filtrate as determined by means of the filtration method. For the SAP beam, similar as for the REF beam only the four reinforcement bars were placed into the moulds beforehand (Fig. 1C). For these beams, similar as for the PU beam, the reinforcement bars were positioned in such a way that the concrete cover on top of them amounted to 20 mm.

Depending on the self-healing approach under investigation, concrete batches with slightly different properties were prepared to make the concrete beams. As vibration with a needle would not be possible for the PU beam, due to the network of wires with capsules, it was chosen to use self-compacting concrete (SCC) for all beams. The composition of each of the concrete mixes is shown in Table 2, together with the flow, air content, density and strength of the concrete. All components were mixed in a 200 L mixer. The mixing procedure was as follows: sand, gravel, cement, limestone filler (and dry SAPs) were mixed properly and homogenously. Subsequently, the needed amount of water was added under continuous mixing. After 1 min of mixing polycarboxylate superplasticizer (concentration 35%) was added steadily while mixing persisted. Fresh concrete properties such as flow, air content and density were measured for each mix immediately after the mixing procedure was finished. Subsequently, the moulds were filled. While part of the concrete mix was used to fill three 150 mm side cubes for determination of the density of the hardened concrete and 28-day compressive strength, most of it was used to fill the moulds of the beams having dimensions of 150 mm × 250 mm × 3000 mm (150 mm is beam height, 250 mm is width of the beam). While the moulds of the cubes were placed in an air conditioned room (temperature 20 ± 2 °C, >90% relative humidity), the moulds of the beams were covered with plastic foil after casting and stored in a standard laboratory climate. Cubes were demoulded after one day and the moulds of the beams were removed after 6 days. After demoulding, cubes and beams were restored, respectively, in the air conditioned room (temperature 20 ± 2 °C, >90% relative humidity) and in the laboratory until the time of testing.

3. Methods

3.1. Four-point bending test

In order to create multiple cracks in the concrete beams, they were loaded in four-point bending. To simplify performance of the water ingress measurements (see Section 3.3), beams were loaded in upward direction (Fig. 2). The metal rollers, used to exert the line loads, were placed symmetrically with regard to the middle of the beam and with a distance in between of 1000 mm. The rollers, representing the supports, were positioned at the ends of the beam. For one of both supports the displacement was fixed in all directions, while the other one was positioned in such a way that movement in x-direction was possible. To make sure that the exerted load was exactly the same for each loading roller and that the load increased at the same speed for both rollers, one jack was used and the force exerted by this jack was transmitted to both rollers by means of a metal beam (Fig. 2). The exerted force

Table 1
Approaches under investigation.

Description	Code
Reference beam without self-healing properties	REF
Beam containing encapsulated polyurethane	PU
Beam containing super absorbent polymers	SAP

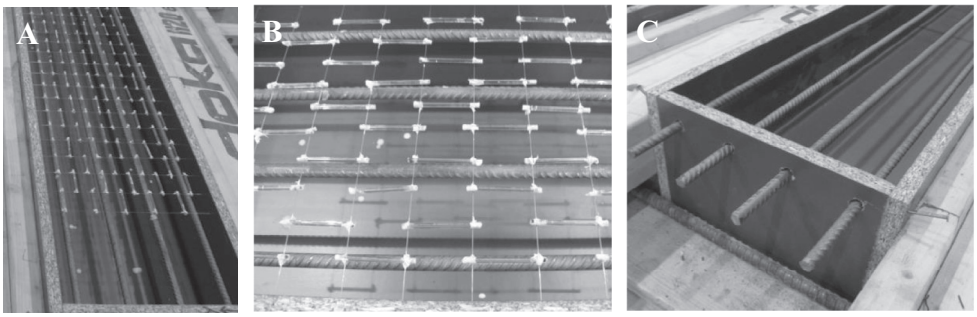

Fig. 1. Preparation of beams with self-healing properties. (A) Placement of glass capsules with embedded polyurethane onto network of wires. (B) Arrangement of the capsules on the wires. (C) Position of the reinforcement bars within the mould.

Table 2
Composition and properties of the concrete mixes (– = not applicable, NA = not available).

	REF		PU		SAP	
Composition						
Components	[kg/m^3]	[l/m^3]	[kg/m^3]	[l/m^3]	[kg/m^3]	[l/m^3]
Sand 0/5	853	–	853	–	853	–
Gravel 2/8	370	–	370	–	370	–
Gravel 8/16	328	–	328	–	328	–
CEM I 52.5 N	300	–	300	–	300	–
Limestone filler	300	–	300	–	300	–
Water	–	165	–	165	–	207
Glenium 51	–	3.33	–	3.00	–	12
SAP	–	–	–	–	3	–
Fresh concrete properties						
Flow	[mm]		[mm]		[mm]	
	680/700		690/660		650/670	
Air content	[%]		[%]		[%]	
	2.4		NA		2.9	
Density	[kg/m^3]		[kg/m^3]		[kg/m^3]	
	2369		NA		2288	
Hardened concrete properties						
Density	[kg/m^3]		[kg/m^3]		[kg/m^3]	
	2314 ± 5		2322 ± 11		2219 ± 8	
Compressive strength	[N/mm^2]		[N/mm^2]		[N/mm^2]	
(28 days)	58.4 ± 0.9		59.2 ± 0.4		47.7 ± 0.6	

was measured with a load cell which was placed in between the metal beam and the jack. The curvature of the beam was measured during four-point-bending by means of five linear variable differential transformers (LVDTs), which were positioned at the bottom side (compressive zone) of the beam (Fig. 2). With regard to the coordinate system shown in Fig. 2, the LVDTs were placed at the following *x*-positions: LVDT_1 at 0 mm, LVDT_2 at 800 mm, LVDT_3 at 1500 mm, LVDT_4 at 2200 mm and LVDT_5 at 3000 mm. As crack healing depends on the crack width and as we want to compare the healing efficiency of the beams with and without self-healing properties, the average crack width was used as reference value during performance of the four-point bending test. Therefore, a measurement frame with a length of 1400 mm was positioned at the top of the beam (tensile zone),

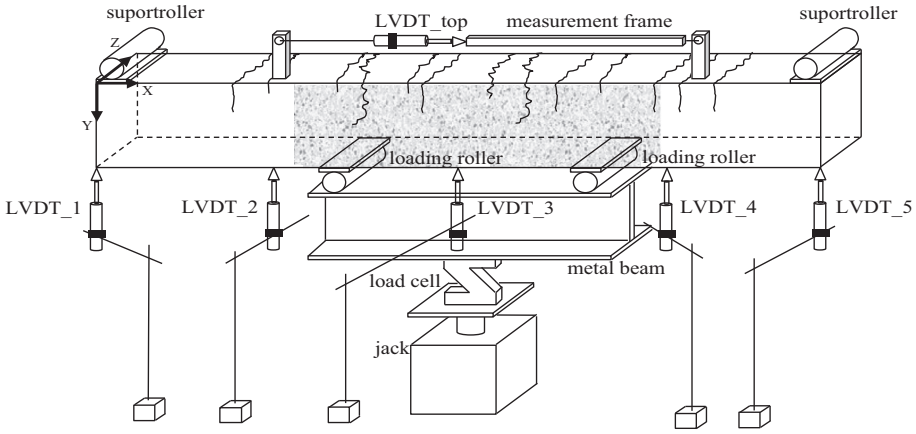

Fig. 2. Test setup of the four-point bending test.

symmetrically with respect to the middle (Fig. 2). The total displacement within the area covered by this measurement frame was measured by an LVDT (LVDT_top), which was connected to the frame in horizontal position. The measured displacement was mainly covered by the formation of cracks and further crack opening and partly by elongation of the concrete matrix. Supposing that the contribution of concrete elongation is rather limited, the value measured by this LVDT represents the total crack opening within the zone covered by the measurement frame. Division of this value by the total amount of cracks seen within this zone, results in the average crack width.

At the moment of crack creation, beams were loaded in four-point bending until the average crack width amounted to 250 μm. Once this value was reached, the average crack width and the deformation of the beams was fixed and the jack and load cell were taken away during the period of crack healing. After a healing period of 7 weeks, the accessories used to fix the crack width and the deformation of the beam were removed after the jack and load cell were installed again. This time, the jack was used to unload the beams. While it was our initial aim to unload the beams partially until the average crack width amounted to 150 μm, unloading was interrupted earlier as plastic deformation occurred. Even at complete unloading, the beams remained partly in their curved position and the average crack width at that time was still higher than the 150 μm we were aiming for. Therefore, it was decided to unload the beams completely (corresponding average crack width for each beam will be reported later). After unloading, the beams were loaded again to see whether crack healing resulted in partial recovery of the mechanical properties. This time the beams were loaded until the average crack width amounted to 300 μm. When this value was reached and kept constant for some minutes, the beams were partially unloaded until an average crack width of 250 μm. In this way water permeability tests could be performed again while the test results could be compared with the ones obtained immediately after crack formation and the ones after crack healing. This would allow to study whether the healing agent within the cracks survives when cracks reopen.

The crack pattern obtained due to loading (until 250 μm), unloading, loading (until 300 μm) and partial unloading (until 250 μm) was visualized. Therefore, each beam was divided in four zones over the length of the beam and the coordinates of the start and end of each crack were determined in relation to the coordinate system shown in Fig. 2. Each crack was named by the number of the zone (I–IV) it was situated in, followed by a letter mark.

3.2. Digital image correlation and acoustic emission analysis

Two advanced monitoring techniques were applied during the four-point bending tests namely digital image correlation and acoustic emission. Digital image correlation (DIC) was considered to visualize the crack pattern on the concrete surface. Two couples of stereoscopic CCD-camera systems were placed side by side and alongside the beam. Each couple of high resolution cameras faced the side view of the beam and periodically captured images of an area which was 600 mm wide and 150 mm high. This side area was covered with a black-white speckle pattern as shown in Fig. 2. The gray-intensity analysis of the speckle-patterned area for a series of images captured during the four-point bending test provided the deformation and strain distribution across the side of the beam. In this study, the strain profiles ε_{xx} (standing for the strain obtained in the direction (xx) parallel to the beam's length) visualized the cracks formed within the covered area (1200 mm × 150 mm).

In addition, eight acoustic emission transducers (with resonant frequency of 150 kHz) were attached on the concrete surface to capture the acoustic emissions released by crack formation (and capsule breakage) during the four-point bending test. The transducers were fixed at the positions shown in Table 3 by using vaseline coupling agent and magnetic holders. The transducers were distributed at all four sides of the beam surrounding the Digital Image Correlation speckle pattern and covering the area where cracks due to bending were expected. The AE analysis considered the attenuation phenomenon (0.05 dB/mm) and a capturing threshold was introduced (hit's amplitude >45 dB). All AE setup features are shown in Table 4. The velocity of the wave propagation was not influenced by the presence of glass capsules as it was measured to be 4000 m/s for both the REF and PU beam (before crack formation). AE analysis considered the total hit and event activity and aimed to clarify the conditions under which cracks form, propagate and close after healing but also to detect activation of the healing mechanism (capsule breakage). The multiple cracking phenomena and the strengthened effect of wave attenuation appeared to deteriorate the accurate wave source localization and to decrease the number of events detected. For the aforementioned reasons, only the analysis of the acoustic emission hits was considered.

3.3. (Improved) autogenous and autonomous crack repair

For the beam with encapsulated polyurethane, crack creation triggered breakage of the capsules, release of the healing agent and subsequent crack repair. For the other self-healing approach under investigation, contact of the cracked concrete beam with water is needed in order to activate the healing mechanism. As contact with water also promotes autogenous healing, the natural mechanism of crack healing which is inherent to concrete, it was decided to bring all beams (REF, PU and SAP) in the same way in contact with water. In this way all beams would exhibit autogenous crack healing to some extent and this effect is filtered out when results are compared mutually. Bringing the beams in contact with water to obtain autogenous healing and to activate the approach with SAP, was done by spraying the beams with water four times a day during 1 min for a time span of 6 weeks (last 6 weeks within the 7 weeks healing period). Therefore, a plastic tube containing holes divided over the complete length of the tube was positioned in the middle above each of the beams. At certain

Table 3
Coordinates of the acoustic emission transducer positions.

Transducer	Coordinates [mm]		
	X	*Y*	*Z*
AE_1	1100	150	125
AE_2	790	75	0
AE_3	1000	0	140
AE_4	1520	20	0
AE_5	1500	150	230
AE_6	2050	0	125
AE_7	2210	75	0
AE_8	1900	150	125

Table 4
AE-testing setup features.

Threshold	45 dB
Pre-amplifier gain	40 dB
Analog filter	
Lower	100 kHz
Upper	2 MHz
Waveform	
Sample rate	1 MSPS
Pretrigger	256
Length	1 k

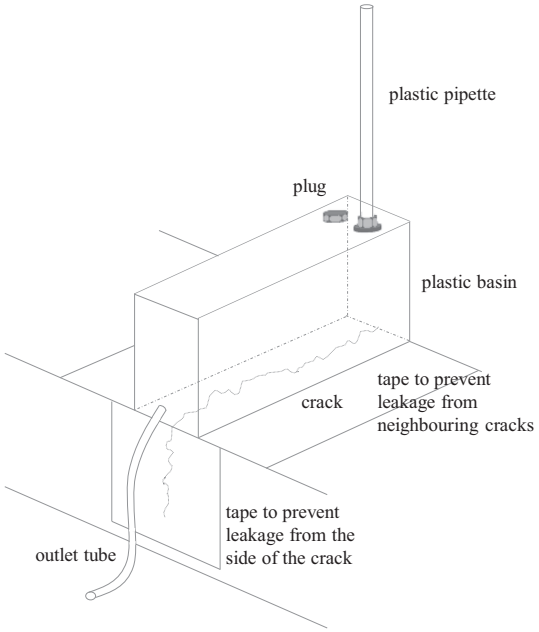

Fig. 3. Test setup used to measure the water ingress.

times, water was pumped through the tubes so it was sprayed on the top and subsequently flowing along the side surfaces of the beams.

3.4. Water ingress measurements

In order to measure the water ingress into the cracks before and after healing and after reloading of the healed cracks, test setups as shown in Fig. 3 were attached on top of the beams. The water basins had inner dimensions of 50 mm × 100 mm × 150 mm. Two holes were provided in the top of each basin. In one opening, a plastic pipette with an inner diameter of 12 mm was positioned. The second hole served to fill the basin with water and was sealed with a plastic plug during performance of the test. While for each beam three basins were glued over one of the selected cracks, the fourth basin was glued in the uncracked zone of the beam and served as a reference. When both, the basin and the pipette, were completely filled with water, the time needed for the water level to move from the indicated mark at the top of the pipette to the one at the bottom, due to water ingress into the crack/beam, was measured. The water ingress was calculated according to Eq. (1):

$$k = \frac{a \cdot T}{A \cdot t} \cdot \ln\left(\frac{h_0}{h_f}\right) \quad (1)$$

where k = water ingress [m/s], a = cross-sectional area of the pipette [m^2], A = contact area between water in reservoir and cracked beam [m^2], T = height of the beam [m], t = time [s], h_0 and h_f = initial and final water head [cm].

Water ingress measurements were performed onto the unhealed cracks, immediately after crack formation, onto the healed cracks, just before reloading of the beams, and a last time on the healed cracks after they had been reloaded.

3.5. Crack width reduction over time measured by optical microscopy

The initial width of each crack was measured at different positions by means of optical microscopy. For each crack, along the whole length of the beam, crack width measurements were performed at 9 positions: 2 measurements at each side of the beam and 5 more measurements at the top surface of the beam. Crack width measurements were performed a second time, at the same positions, after the 7 weeks healing period to allow calculation of the crack width reduction over time.

3.6. X-ray tomography analysis of drilled cores

After completion of the reloading test, beams were taken from the test setup and cores with a diameter of 50 mm were drilled over the complete height of the beams. Locations for core drilling were chosen in such a way that each core covered a crack. Afterwards, one core of each beam was scanned at the Centre for X-ray Tomography of the Ghent University (UGCT) [16] using the X-ray micro-tomography (μCT) cone beam setup of the HECTOR scanner [17]. Each sample was scanned stack-wise in 4 consecutive scans in order to cover the full height of 150 mm of each core. For each scan, a total of 3001 projections was acquired over an angle of 360°, with an exposure time of 1 s per projection. A cupper filter of 0.5 mm thickness was employed to block low-energetic X-rays at the source to reduce beam hardening. 24 dark-field (no X-ray beam) and 48 flat-field (no sample) images were acquired, in order to correct for inhomogeneities of the detector and X-ray beam. The X-ray tube provided a voltage of 200 kV with a power of 30 W. The source-detector distance was 1167 mm and the source-object distance 178 mm, resulting in a voxel size of 30 μm. After the acquisition, the raw data were reconstructed using the in-house developed software [18]. The same set of parameters for ring and spot removal, tilt and skew of the detector and beam hardening were adopted for all scans.

3.7. Fluorescent microscopy and thin section analysis of drilled cores

In addition, 50 mm diameter cores, with a crack inside, were obtained from each of the beams for further investigation by means of fluorescent microscopy. For each type of concrete beam two cracked cores were vacuum impregnated with fluorescent epoxy while being placed inside a PVC tube. After hardening of the dye the cores (and tubes) were sawn in longitudinal direction. While one half was used for analysis of the crack under fluorescent light, the other half was used for further preparation of thin sections. Therefore, a sample of approximately 50 mm × 30 mm × 20 mm was cut from the upper part (covering the crack) of the second half of the concrete cores. The cut sample pieces were then glued onto 30 mm × 50 mm glass plates, cut to a thickness of 10 mm and plane grinded. Samples were then cleaned and dried for 1 h. Subsequently, samples were placed in a vacuum chamber for 2 h after which fluorescent epoxy was added. After being removed from the vacuum chamber, the impregnated samples were placed in between two pieces of strong plastic film for 15 h. Afterwards samples were grinded to remove excess epoxy and 0.01 mm of the concrete surface. Then the grinded surface was glued onto an object glass and the samples were cut as close as possible to the object glass leaving an approximately 0.3 mm thin impregnated concrete slice. This slice was then further grinded to a thickness of 20 μm after which a cover glass was glued onto it with UV hardening glue. The thin sections were subsequently analyzed by means of light microscopy with polarized and non-polarized light.

Table 5
Average crack width at the end of crack creation.

Beam	# Cracks in middle zone [–]	Elongation of middle zone [mm]	Average crack width [μm]
REF	20	4.01 + 1.10	256
PU	22	4.00 + 1.55	252
SAP	24	5.94	248

4. Results

4.1. Multiple crack formation

The aim of this study was to investigate whether an improved crack healing efficiency was obtained for the beams with the implemented self-healing approaches (PU and SAP) compared to the reference beam (REF). As the crack healing efficiency, particularly the contribution of autogenous healing, largely depends on the crack width, we aimed for a similar crack width for all of the beams under investigation. Each beam was loaded until an equal average crack width of 250 μm was reached. In Table 5 it can be seen that the number of cracks within the zone covered by the measurement frame (Fig. 2) differed for each of the beams, being 20, 22 and 24 for the REF, PU and SAP beam, respectively. It was expected that the highest amount of cracks would be obtained for the SAP beam as this concrete matrix had the lowest strength (see Table 2) and as the SAP particles act as flaws and thus stress initiators [19]. As the amount of cracks was different, the loading and thus also the elongation of the beams within the middle zone differed. For the REF beam and the PU beam, the elongation in the middle zone is represented as the sum of two values as the loading was performed in two stages. However, for each of the beams the average crack width (obtained by dividing the total elongation in the zone covered by the measurement frame (Fig. 2) by the number of cracks within that zone) amounted to approximately 250 μm. It can be seen from Fig. 4 that similar crack patterns developed for the REF, PU and SAP beam. A more dense crack pattern was observed in the middle of the beam (zone II and III), while less cracks were seen when moving closer towards the supports (zone I and IV). In addition to a visualization of the crack pattern at the top and at one side of the beam, a visualization by use of ε_{xx} DIC profiles of the cracks at the other side of the beam is given in Fig. 4. For each beam the presented profile corresponds to the profile obtained at the end of loading for the first and the second DIC system, respectively.

In Fig. 5 the vertical displacement measured by the LVDTs positioned along the length of the beams is given. For the REF beam and the PU beam, the displacement is shown as the sum of two bars as these displacements were obtained in two separate loading stages. It can be clearly seen that for LVDT_1 and LVDT_5, which were placed close to the supports, the measured displacement was very

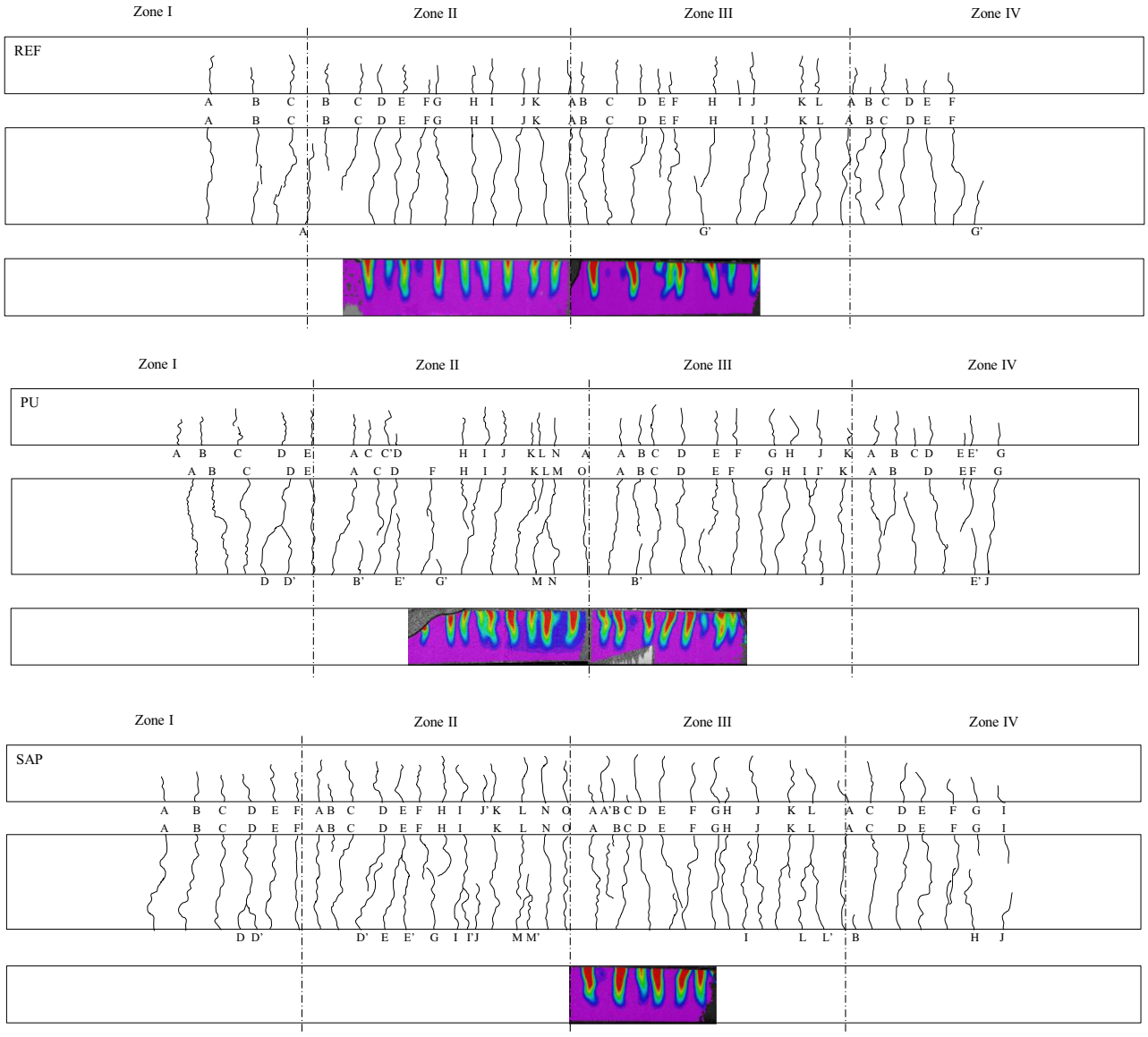

Fig. 4. Visualization of the crack pattern at the top and the sides of the beam. For one side of each beam the crack pattern is visualized by the obtained DIC profiles at the end of crack formation (left hand side of DIC profile for SAP beam is missing).

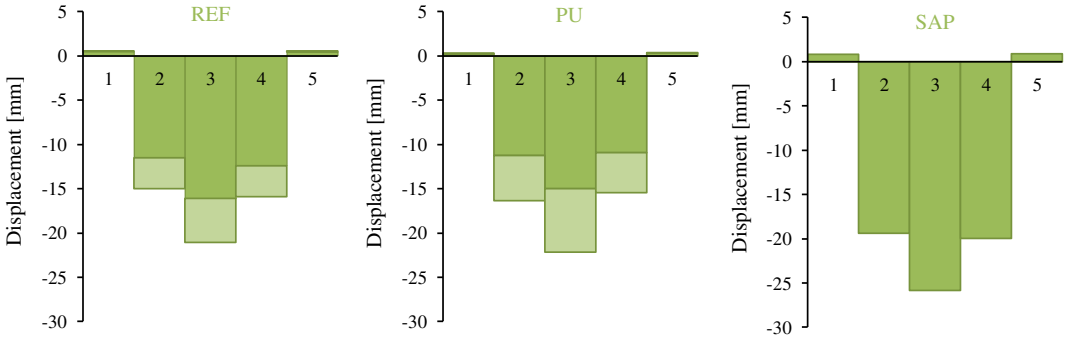

Fig. 5. Vertical displacement of the beams measured during crack formation at the position of LVDT_1, LVDT_2, LVDT_3, LVDT_4 and LVDT_5.

little, as expected. For LVDT_2 and LVDT_4, placed symmetrically with regard to the middle of the beam, a similar negative value for the displacement was measured (*y*-axis oriented downward (Fig. 2)). The highest negative value was seen in the middle of the beam (LVDT_3). Since for the SAP beam more cracks were detected in the middle zone, and thus loading was continued to obtain the same average crack width, higher absolute values for the displacement were registered. While for the REF beam and the PU beam the displacement in the middle of the beam amounted to −20.76 mm and −22.91 mm, for the SAP beam this value amounted to −25.84 mm. This was also noted when comparing the load at the end of crack formation for each of the beams. While for the REF and the PU beam the registered total load was around 36 kN, for the SAP beam a value of around 42 kN was noted. This does not imply that the SAP beam has better mechanical properties compared to the other beams (in fact the opposite is true). The higher final load of the SAP beam is caused by the fact that the SAPs act as crack initiators so more cracks are created in this beam and loading needs to be continued longer in order to obtain the same average crack width.

After crack formation and crack healing for 7 weeks, the beams were unloaded. The average crack width (obtained by dividing the total elongation in the zone covered by the measurement frame (Fig. 2) by the number of cracks within that zone) at the end of unloading amounted to 182 μm, 210 μm and 160 μm for the REF, PU and SAP beam, respectively. The fact that the resulting average crack width for the PU beam was obviously higher could serve as a proof that the cracks of this beam were filled with hardened polyurethane.

After this unloading cycle beams were loaded again (until average crack width of 300 μm) to verify whether the mechanical properties were (partially) recovered due to crack healing. In Fig. 6 the deflection measured by LVDT_3 is plotted against the increase in load registered upon reloading. However, based on these graphs no sound conclusions can be taken regarding the recovery in mechanical properties as similar curves are obtained for each of the beams. Again, the load registered for the SAP beam is highest but this is due to the higher crack density. It should be noted that from previous experiments on lab-scale it was proven that self-healing due to both approaches, embedment of encapsulated polyurethane and addition of SAPs to the concrete, led to partial regain of the mechanical properties. The fact that this is not seen in the current large-scale test could be attributed to the fact that part of the released or precipitated healing agent was destroyed upon unloading of the beams.

4.2. Detection of healing activation by using acoustic emission hit activity

As previously done on small-scale test samples [20,21], activation of the self-healing approach based on encapsulated polyurethane was confirmed by means of acoustic emission analysis. Based on an energy-analysis, a discrimination could be made between hits obtained due to crack formation and capsule breakage. Every time a capsule breaks or a crack forms, each of the AE transducers captures a waveform, represented by a set of descriptors which were analyzed in this study. Thereby, the AE hit's energy, derived from the area under the waveform shape, is indicative to the released fracture energy and its magnitude and general characteristics are indicators of the damage mode. High energy hits corresponded to discrete events of capsule breakage and were well differentiated from the rest of the AE events. Only in the case of capsule breakage, the energy received by all the eight transducers placed at the surface of the beam exhibited values ranging from

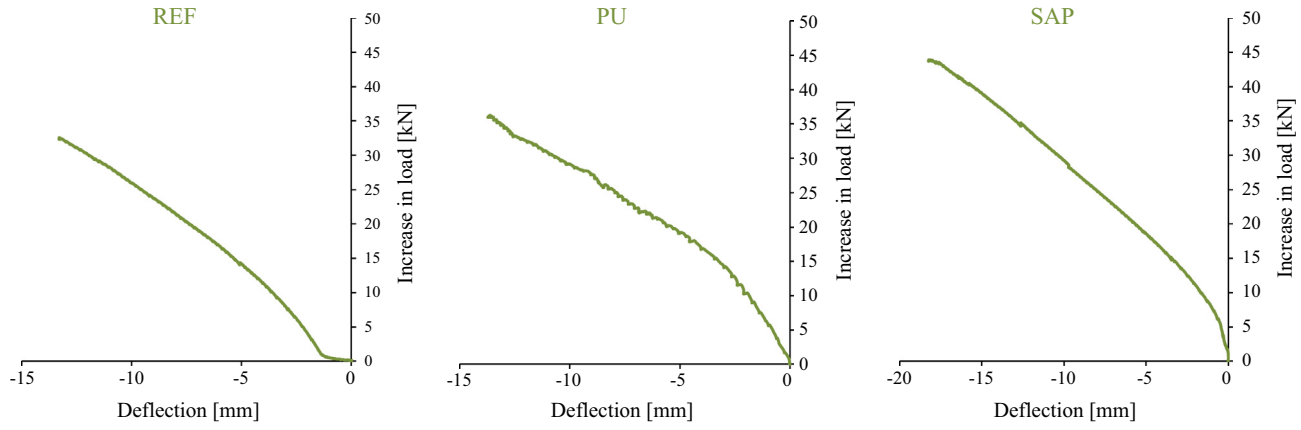

Fig. 6. Deflection measured by LVDT_3 in function of the increase in load registered during reloading until 300 μm average crack width.

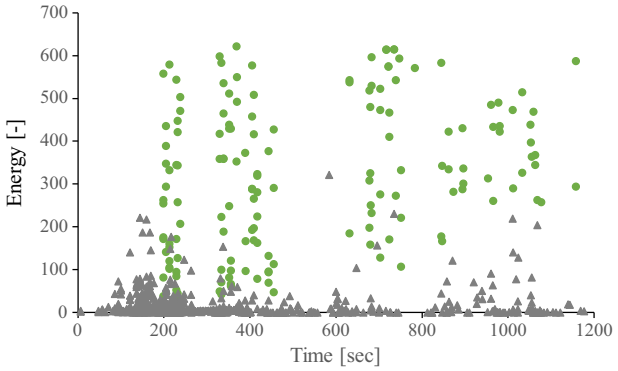

Fig. 7. Clustering of AE hits activity on real scale concrete beams tested under four-point bending. Green dots represent hits due to capsule breakage, gray triangles represent hits due to crack formation. (For interpretation of the references to color in this figure legend, the reader is referred to the web version of this article.)

2000 to 12,000 depending on the receiver's transducer distance from the event location (the energy of hits is relatively low in case of transducers placed far from the broken capsule and higher in case of transducers standing closer to the broken capsule). Any other AE activity which is captured, is caused by crack formation of the concrete matrix.

In Fig. 7, the hit activity as captured during crack creation is presented. The plot of hits versus time is given and two clusters are presented (the green dots stand for the hits obtained due to capsules rupture and the gray triangles for the formation of cracks within the concrete matrix). The clustering is achieved considering that brittle glass capsule rupture emits instant hits of greater energy compared to hits due to concrete cracking. About 200 s after the beginning of the four-point bending test, the first hits related to capsule breakage are detected. Based on the DIC crack pattern obtained at that time, it seems that capsules start to break when the average crack width is about 50 μm. From 350 until 450 s after the beginning of the test a new series of capsules seems to break. After that no capsule breakages are detected until 650 s after starting. Within the zone covered by the DIC camera system 2.5 cracks/100 mm arose at that time with an average crack width of 100 μm. From that moment on capsule breakage is detected continuously until the end of the loading test. It appears that the healing activation protocol based on AE energy analysis can also be applied on real-scale concrete structures.

4.3. Water ingress measurements

As for the beam containing encapsulated polyurethane (PU) crack formation coincided with triggering of the healing mechanism (capsule breakage and release of the healing agent), the water ingress measurement performed immediately after crack formation takes healing due to release of polyurethane already into account. This is represented by the results shown in Fig. 8A as for the measurements in the cracked zone of the PU beam the lowest water ingress was obtained. The obtained values were lower compared to the values obtained for the REF and SAP beam and in addition these values were somewhat lower compared to the water ingress obtained in the uncracked zone of the PU beam. In Fig. 8 the code of each crack for which the water ingress was measured is noted on top together with the average crack width measured before healing at the top of the beam. It can be seen that for all cracks under consideration the average crack width is within the same range (100–140 μm). It can also be seen from Fig. 8A, that before crack healing, the water ingress into the cracks of the beam with embedded SAPs was clearly higher compared to the ingress into the other series (REF and PU). This could be due to the fact that the SAP particles along the crack faces of this beam attract an additional amount of water filling up the formed macropores. However, this could result in a beneficial effect later on, as the water, absorbed by the SAPs, will be released to the surrounding cementitious matrix and result in further hydration and calcium carbonate precipitation. When these newly formed crystals are precipitated inside the cracks this results in an increased autogenous crack healing efficiency. This improved healing efficiency is partly represented by the results obtained after crack healing and before reloading of the beams (Fig. 8B). While for the REF beam and the PU beam higher water ingress values were obtained after healing of the cracks, the SAP beam showed a lower water ingress for the measuring positions covering a crack. For the measurements performed in the uncracked zone, the values before and after crack healing were more or less the same. We believe that the difference noted for the SAP series should be attributed to healing of the cracks as for the SAP series crack closure was also shown from the microscopic analysis (see Section 4.4). The fact that higher water ingress values were measured for the two other test series (REF and PU) is in contradiction with our expectations. Not too much difference can be seen between the results obtained before or after reloading of the healed cracks (Fig. 8B and C). It should be mentioned that these water ingress measurements were very difficult to perform as for some of the selected cracks water was not only intruding in the concrete matrix via the crack but also leaked out of neighboring cracks. This makes it very difficult to draw sound conclusions from this experiment and thus for future experiments this test setup needs to be improved.

4.4. Visualization of crack closure by microscopy

Due to cyclic exposure of the cracks to water for a period of 6 weeks, they showed some autogenous healing. This is proven as white precipitates, connected to the crack faces, can be detected. In Fig. 9 it can be noticed that for the reference beam (REF) narrow cracks (II F right hand side and IV C (crack width 42 μm)) tend to close completely, while wider cracks (II F left hand side (crack width 126 μm)) show partial crack healing and almost no healing is observed in the case cracks within the REF beam become too wide (II B (crack width 210 μm)). This confirms that the natural, autogenous crack healing mechanism is limited to healing of smaller cracks. From the micrographic representation of crack III D (with a crack width of 63 μm) it becomes clear that healing products start to form from the crack faces and grow towards each other. As soon as precipitates from both crack sides reach each other, complete crack healing is obtained. For some of the wider cracks within the REF beam, the crack faces were connected at some points due to crack healing while at some other points within the same crack almost no healing was noticed (connections indicated with arrows for cracks II B (crack width 210 μm) and II D (crack width 137 μm)). This may be attributed to the fact that further hydration and calcium carbonate precipitation (causing autogenous crack healing) start from the positions along the crack where cement paste is available. This means that disruptions within the healing material will be noted at the positions where the crack crosses sand grains or aggregates.

For the beam with encapsulated polyurethane (PU), the highest portion of crack sealing occurred at the moment of crack formation and capsule rupture. It can be seen from Fig. 9 that even wider cracks could close completely due to release of the embedded healing agent (III I with a crack width of 189 μm). However, it should be mentioned that not for all cracks complete crack filling with polyurethane was noted. As seen for crack IV F (with a crack width of 32 μm) the upper part of the crack is filled with polyurethane healing agent while for the lower part no polyurethane could be detected at the surface but partial filling with calcium carbonate

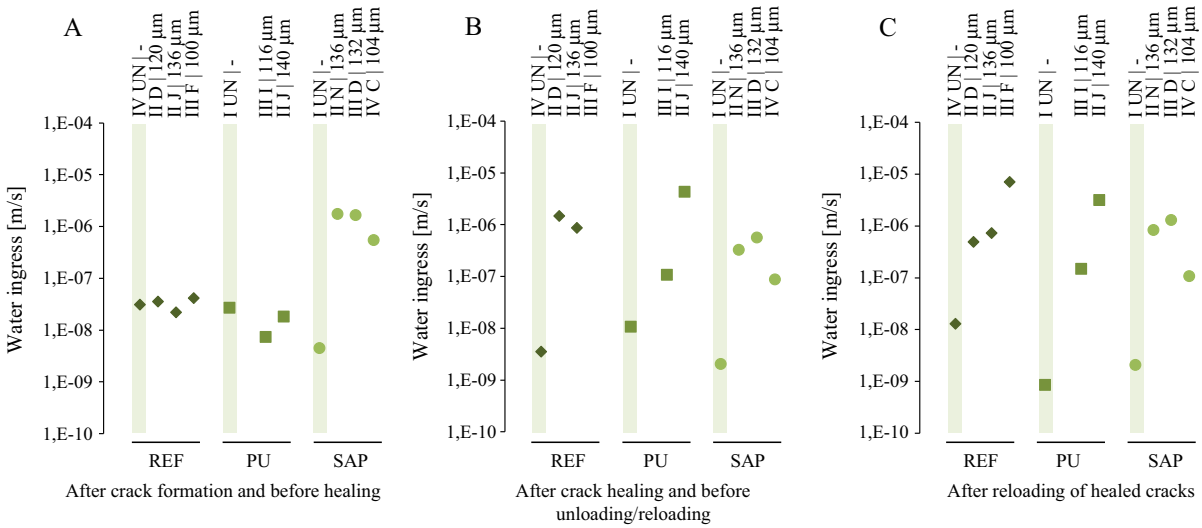

Fig. 8. Water ingress for each test series measured before and after the healing period and after reloading of the healed cracks. Shaded area refers to measurement in uncracked zone (noted as 'zone number UN'). On top of each graph the crack code is given together with the average crack width. At certain time steps some results are missing as for some measuring positions leakages were noted.

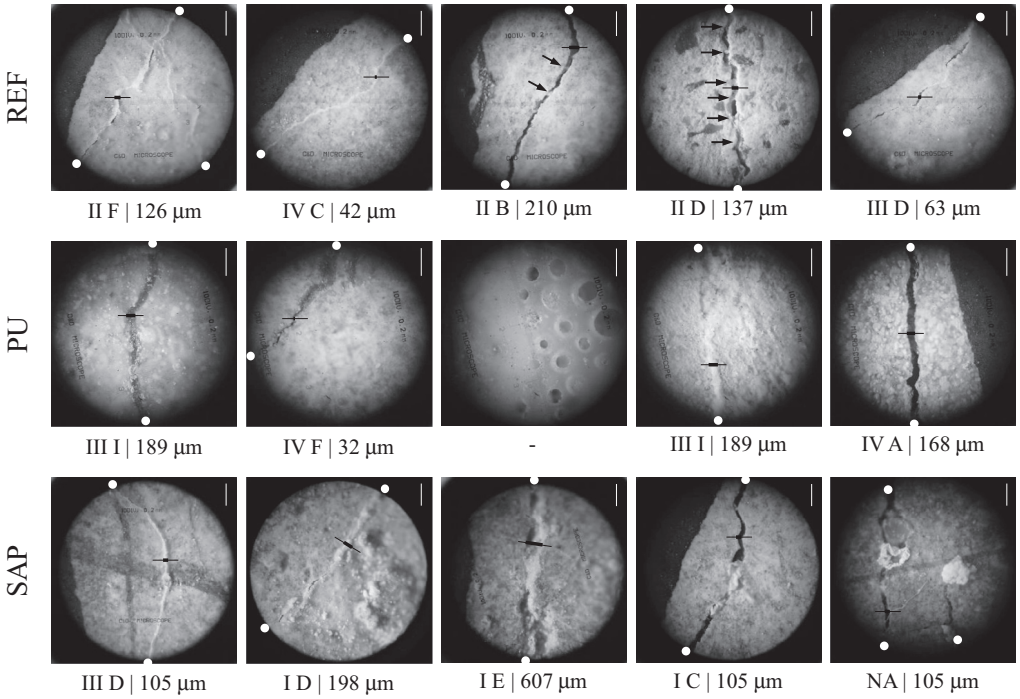

Fig. 9. Micrographs of the (healed) cracks inside the REF, PU and SAP beam. White dots are used to indicate the start and end position of each crack. The length of the white line in each picture represents 500 µm. Under each micrograph the crack code is mentioned together with the crack width measured at the location indicated in the micrograph with the following black symbol: -■- ('NA' = crack code not available, '–' = crack code and crack width not applicable).

crystals can be noted. In the next picture a spot of leached polyurethane is shown to make clear that this one component agent foams upon contact with the air. Due to the 6 weeks spraying with water of the PU beam not only autonomous crack healing occurred but in addition some autogenous healing closed the cracks. Similar as for the REF beam part of the cracks showed complete healing (III I with crack width of 189 µm) while other cracks only showed partial healing (IV A with crack width of 168 µm).

For the beam with superabsorbent polymers, improved crack healing was noticed compared to the REF beam. This can be clearly seen in Fig. 9. While for the medium sized cracks (III D with a crack width of 105 µm) complete crack filling is noticed, for cracks with larger widths (I D (crack width 198 µm)) almost complete crack filling by precipitates can be seen but still some gaps are detected. For this test series also wide cracks (I E (crack width 607 µm)) show crack healing to a certain extent. So for the SAP beam more complete crack healing was obtained and also larger cracks could be more completely filled. In the last two pictures of Fig. 9 spots are shown where clusters of SAP were present absorbing and releasing water during the spraying periods and thus resulting in the formation of a cluster of calcium carbonate particles.

In addition to a visual evaluation of the crack closure efficiency, a quantitative analysis of the crack healing efficiency in function of the crack width was performed. The crack closing ratio was

calculated as the difference in crack width before and after healing divided by the original crack width. This evaluation procedure only takes into account the amount of healing obtained during the 6 weeks showering period and not the extent of immediate healing of the beam with encapsulated polyurethane (PU). Cracks were divided into different categories, based on the original crack width, and crack closing ratios were calculated for each category of each test series. What immediately can be seen from Fig. 10 is that smaller cracks are more likely to be healed compared to wider cracks. For crack widths within the range of 0–50 μm, crack closing ratios within the range of 40–80% were obtained, while for the cracks within the largest crack width range (200–250 μm), ratios only amounted to 10–30%. A gradual decrease of the sealing ratio for each test series can be seen with increasing crack width range. A second very clear finding is that the sealing ratio for the beam with embedded SAP particles (SAP) is considerably higher compared to the sealing ratios which are obtained for the two other test series under investigation (REF and PU, having almost the same sealing ratios for each range).

This finding clearly indicates that the addition of SAPs to the concrete matrix promotes autogenous crack healing when the crack faces are exposed to water. Due to the addition of SAPs, a sealing ratio of 80% was obtained for cracks within the smallest crack width range. But also for the largest range, about 30% healing was obtained after 7 weeks, when SAPs were added to the matrix. Although no improved sealing ratio is noticed when the PU beam is compared with the REF beam, this does not mean that healing was inefficient for this series. The healing efficiency of the PU beams is just not reflected by this experiment as at the time of the initial crack width measurement, autonomous healing already occurred for the PU beam. This experiment only shows the amount of additional autogenous crack healing which occurred during the 7 weeks healing period with 6 weeks showering.

4.5. X-ray tomography analysis of drilled cores

A selection from the upper part (top 45 mm) of each core, which was obtained after unloading and reloading of the beams, was visualized in 3D. The visualization of the reference sample (REF) starts approximately 3 mm below the upper surface and is approximately 22 mm high (Fig. 11A). The visualized volume of the sample with SAPs starts approximately 5 mm below the upper surface and has a height of approximately 27 mm (Fig. 11B). The visualizations show a clear difference in porosity between the REF and the

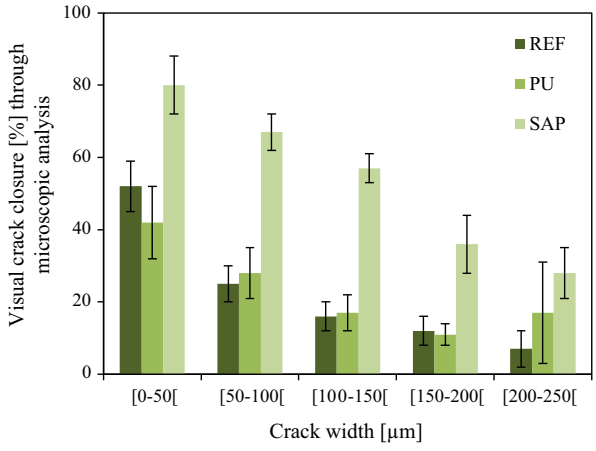

Fig. 10. Crack healing ratio obtained within each crack range and for each of the test series under investigation.

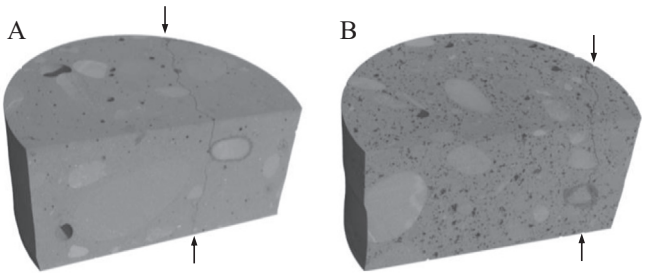

Fig. 11. 3D visualization of the core (diameter 50 mm) obtained, after unloading and reloading of the beams, from (A) the REF beam and (B) the beam with SAP. The start and the end position of the crack is indicated with an arrow. The core of the REF beam was obtained from crack III D (mean crack width at top of beam 144 μm) and the core of the SAP beam from crack IV H (mean crack width at top of beam 43 μm).

SAP sample, illustrating that SAPs tend to result in the formation of macro-pores in which SAP particles are located. As it can be seen from Fig. 11B that the created crack crosses several of these pores, it is most likely that water entering a crack within the SAP beam will be blocked by the swelling action of the SAP particles within the pores crossed by the crack. Next to this crack blocking effect, improved autogenous healing by further hydration and calcium carbonate precipitation is expected due to inclusion of the SAPs. However, it is hard to prove this from the reconstructed images shown in Fig. 11 due to the limited resolution. The narrow cracks are only represented by a few voxels within the reconstructed image and therefore it is very difficult to see whether there would be more healing of the crack in the SAP sample compared to the crack in the REF sample. However, what can be derived from these reconstructed images is that for none of the beams complete crack healing was obtained as for both samples the crack colors rather black which means it is still (partially) filled with air instead of healing products. However, it should be noticed, that due to the fact that the cores were obtained after unloading and reloading of the beams, the formed healing products inside the cracks may have been destroyed due to reopening of the crack.

The visualization of the sample containing polyurethane filled capsules is given in Fig. 12A. The distribution of the PU in the crack and the remaining PU inside the capsules are depicted in yellow in the 3D visualizations and the horizontal cross section of this sample (Fig. 12B–D). The 3D volume starts approximately 4 mm below the upper surface and is 30 mm high. The capsules are located at a depth of approximately 13 mm below the upper surface. From Fig. 12A it seems that also for this core the crack tends to color rather black on the reconstruction. However, the crack of this core is expected to be filled with polyurethane which has a low attenuation coefficient for X-rays (contrary to calcite and hydration products which had to fill the crack of the REF and SAP sample) so in this case the presence of a low RGB value within the crack does not mean that the crack is not healed. For this core, it was possible to perform a qualitative analysis of the crack healing potential in the upper part of the sample. The reconstructed dataset was loaded in the in-house developed software [22] and the crack and the capsules were selected. Within this region of interest, the PU was segmented based on its gray values. These were clearly visible in the capsules, where part of the PU remained after crack formation. Due to the limited crack width, gray values of the PU within the crack may overlap with gray values resulting from partial volume effects in the crack. The segmentation of the PU within the crack should thus be considered as an indication for the healing potential, but cannot be used for quantitative assessment. The distribution of the PU in the crack and the remaining PU inside the capsules are depicted in yellow in the 3D visualizations and the horizontal cross section of this sample (Fig. 12B–D). In

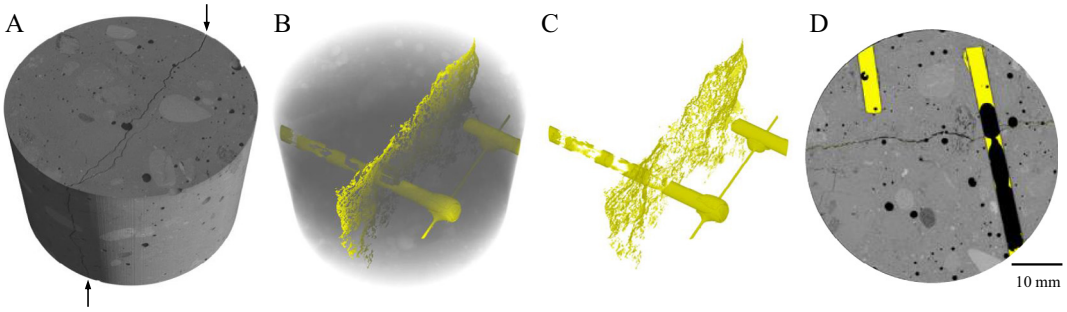

Fig. 12. 3D visualization of the core (diameter 50 mm) obtained from the PU beam with start and end position of the crack indicated with an arrow (A), the core obtained from the PU beam with in yellow the volume which represents the PU that filled the crack or remained in the capsules (B), the PU that filled the crack or remained in the capsules (C). Horizontal cross section at the capsule height in which the yellow color represents PU that filled the crack or remained in the capsules (D). The core of the PU beam was obtained from crack III E (mean crack width at top of beam 156 μm). (For interpretation of the references to color in this figure legend, the reader is referred to the web version of this article.)

Fig. 12B and C the healing agent remaining within one complete and one partial capsule is shown. The line connecting both capsules in Fig. 12B and C represents the plastic wire which was used to position the capsules within the mould. It became part of the region of interest and also colored yellow as it has a similar attenuation coefficient as polyurethane. It can be seen from Fig. 12B and C that quite some healing agent remained inside the capsules. From this it could be concluded that less capsules or shorter capsules could be used in order to obtain as much crack filling as was seen during this experiment. However, a lower amount of capsules or the use of shorter capsules would also decrease the chance a crack crosses the capsules and could thus lower the crack healing efficiency. Although the capsules are not completely empty, it can be seen that over the complete visualized volume polyurethane is present within the crack. It did not form a continuous layer but seemed to spread inside the crack and cure with some air gaps in between. These findings are confirmed when considering the cross-section shown in Fig. 12D.

4.6. Fluorescent microscopy and thin section analysis of drilled cores

In Fig. 13 one half of the concrete cores obtained from each of the beams after unloading and reloading, is shown when being placed under fluorescent light. For each of the samples, the crack ran over more than half the height of the beam. While for the specific core of the REF beam shown in Fig. 13 the crack has a depth of 89 mm, for the SAP and the PU beam these values amounted to 93 mm and 106 mm, respectively. The second conclusion which can be drawn is that none of the cracks is completely closed due to (improved) autogenous or autonomous crack healing as illumination of the fluorescent dye inside the crack is clearly noticed. However, it can be seen that for the beam with embedded capsules the upper 23 mm did not seem to be impregnated. This becomes even clearer when looking at the magnification of zone III shown at the right hand side of Fig. 13. This proves that the upper part of the crack was sealed due to release of polyurethane after crack formation and capsule breakage. Although from the X-ray

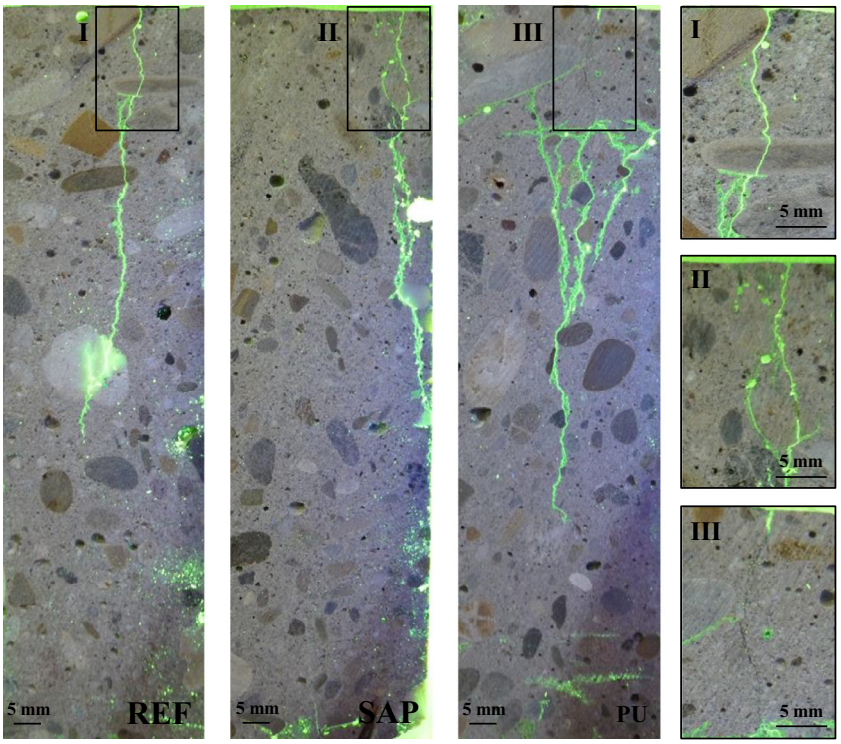

Fig. 13. Picture of cracked concrete cores, obtained after unloading and reloading of the beams, placed under fluorescent light. The crack width at the crack mouth amounted to 120 μm (REF), 6 μm (SAP) and 160 μm (PU). At the right hand side an enlargement of the top of the crack is shown (I–III).

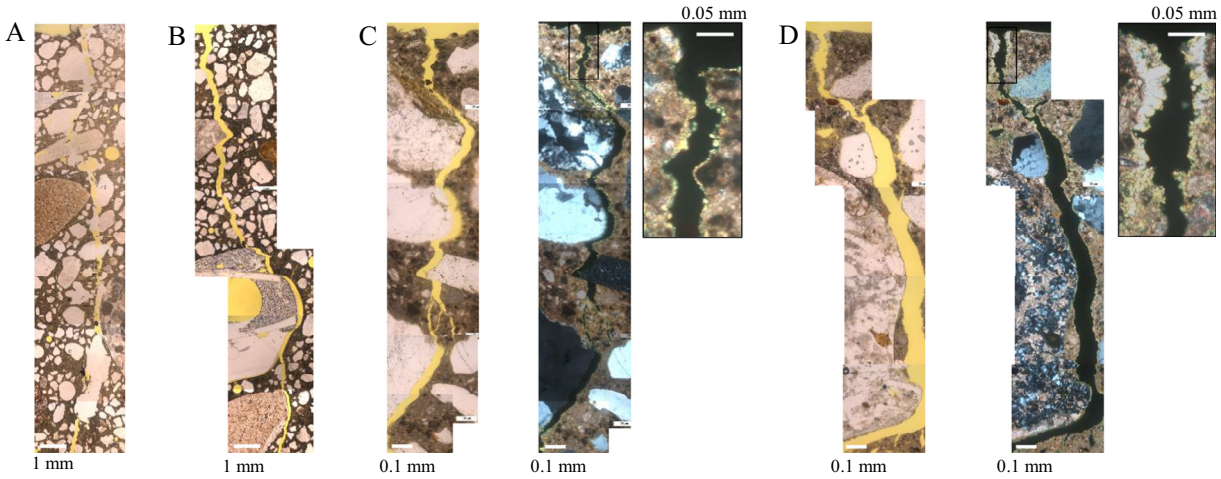

Fig. 14. Analysis of thin sections obtained from the PU (A and B), REF (C, left: non-polarized and middle: polarized light) and SAP (D, left: non-polarized and middle: polarized light) beam after unloading and reloading. A magnification of the zone corresponding to the crack top (indicated with a black rectangle in pictures C and D) is shown at the right.

tomographic analysis it was shown that no continuous layer of polyurethane was obtained inside the crack, from the analysis of the cores under fluorescent light it seems that even this discontinuous layer can prevent the ingress of epoxy and will thus also prevent the ingress of aggressive agents.

Due to the fact that the concrete cores used for thin section preparation were obtained after unloading and reloading of the beams, closure and further widening of the cracks partially destroyed the formed hydration products and crystals inside the crack, creating a pathway for the fluorescent dye in case of the REF and the SAP beam. For the PU bam this was not the case as cracks were filled with a flexible type of PU, able to withstand the crack closure and reopening upon unloading and reloading.

Similar conclusions can be drawn when analyzing the thin sections by light microscopy. Thin sections were taken after reloading of the beam, thus further crack opening has ruptured especially the brittle calcium silicate hydrates and calcium carbonate healing products. For the section shown in Fig. 14A which is obtained from the beam with encapsulated polyurethane, it can be seen that up to a certain depth the crack is filled with polyurethane. However, for the sample shown in Fig. 14B, which was also obtained from the PU beam no crack healing was noticed. This is due to the fact that in this case the crack ran around the capsule and no polyurethane could leak into the crack to heal it. This explains the results obtained for the water permeability test. The reduction in water ingress was limited as only some of the created cracks seemed to heal while other cracks did not cross any embedded capsules and thus remain unhealed. The most important aim of this thin section analysis was to detect until what depth calcium carbonate crystals could be noted within the autogenously healed cracks of the REF and the SAP beam. In Fig. 14C and D one crack of the REF and SAP beam is shown under polarized and non-polarized light. It can be noticed that for both test series more crystal precipitation is seen closer to the crack mouth. Another finding is that the precipitation is limited to the crack faces and that less precipitation could be seen inside the crack. Due to reloading of the beams the precipitated healing products were destroyed so they could not be detected anymore by the thin section analysis.

5. Conclusion

From this study it can be concluded that both self-healing approaches under investigation have some potential to be applied on real scale. However, the use of encapsulated polyurethane requires much more preparation to fill the tubes and position them in the moulds compared to the addition of SAPs. Therefore, current research focusses on the development of encapsulation materials with properties evolving over time. So at first they should be flexible and survive concrete mixing while later on the capsules should become very brittle to break at the moment of crack formation. Use of this type of capsules would strongly decrease the time needed for preparation of concrete elements containing encapsulated healing agent. This is subject to further research. In this study, however, as the capsules were positioned manually into the mould, they were oriented perpendicular to the expected crack direction which results in the highest healing efficiency. When capsules are mixed in, they will be oriented randomly and the healing efficiency will depend on the spatial orientation of the capsules. With regard to the healing efficiency, the approach making use of embedded SAPs seemed to result in the highest healing efficiency based on the crack width reduction measurements. Crack closure was obviously enhanced through the addition of SAPs to the concrete matrix. This was less clear for the beams with embedded polyurethane, however, the healing efficiency of this approach was not reflected by the crack width measurements. While it was hard to prove a good healing efficiency from the water ingress measurements, after crack formation release of polyurethane from the capsules inside the cracks and (partial) crack closure was clearly noticed from the CT, microscopy and thin section analysis.

The approach using encapsulated polyurethane is triggered by crack appearance and thus does not require water to obtain healing. Therefore, this approach can be used for multiple applications such as healing of bending cracks in beams of bridges, healing of thermal cracks in insulated concrete sandwich panels, ... In order to activate the approach based on the SAPs, water is needed to cause swelling of the SAPS and healing by further hydration and calcium carbonate formation. However, from previous research it was shown that water should not necessarily be present in a liquid form. Also cracked samples with embedded SAP exposed to a 90% RH environment seemed to show crack healing, although with a lower efficiency compared to samples exposed to wet-dry cycles [9]. We believe that the main areas of application of this approach are water retaining structures such as swimming pools, underground structures such as tunnels and basements, ... where you have shrinkage cracks. As these structures are expected to be watertight, through going cracks, which cause liquids from to penetrate from the one side to the other side of the structure are really problematic. However by adding SAPs the entering liquids will be

blocked before they reach the other side resulting in a water tight wall and moreover when they release their water content after time they will cause permanent crack healing.

Acknowledgements

This research under the program SHE (Engineered Self-Healing materials) (project SECEMIN: Self-healing cementitious and mineral building materials) was funded by SIM (Strategic Initiative Materials in Flanders). The authors would like to thank SIM for its financial support. Kim Van Tittelboom is a postdoctoral fellow of the Research Foundation – Flanders (FWO) (project number 12A3314N) and acknowledges its support.

References

[1] S.R. White, N.R. Sottos, P.H. Geubelle, J.S. Moore, M.R. Kessler, S.R. Sriram, E.N. Brown, S. Viswanathan, Autonomic healing of polymer composites, Nature 409 (2001) 794–797.
[2] C. Edvardsen, Water permeability and autogenous healing of cracks in concrete, ACI Mater. J. 96 (4) (1999) 448–454.
[3] H.-W. Reinhardt, M. Jooss, Permeability and self-healing of cracked concrete as a function of temperature and crack width, Cem. Concr. Res. 33 (7) (2003) 981–985.
[4] V. Li, E.H. Yang, Self healing in concrete materials, in: S. Van der Zwaag (Ed.), Self Healing Materials: An Alternative Approach to 20 Centuries of Materials Science, Springer Science, Dordrecht, The Netherlands, 2007, p. 388.
[5] A. Jefferson, C. Joseph, R. Lark, B. Isaacs, S. Dunn, B. Weager, A new system for crack closure of cementitious materials using shrinkable polymers, Cem. Concr. Res. 40 (5) (2010) 795–801.
[6] H.X. Dennis Lee, H.S. Wong, N. Buenfeld, Self-sealing cement-based materials using superabsorbent polymers, in: O.M. Jensen, M.T. Hasholt, S. Laustsen (Eds.), International RILEM Conference on Use of Superabsorbent Polymers and Other New Additives in Concrete, RILEM Publications s.a.r.l, Lyngby, Denmark, 2010, pp. 171–178.
[7] D. Snoeck, S. Steuperaert, K. Van Tittelboom, P. Dubruel, N. De Belie, Visualization of water penetration in cementitious materials with superabsorbent polymers by means of neutron radiography, Cem. Concr. Res. 42 (8) (2012) 1113–1121.
[8] D. Snoeck, N. De Belie, Repeated autogenous healing in strain-hardening cementitious composites by using superabsorbent polymers, J. Mater. Civ. Eng. 04015086 (2015).
[9] D. Snoeck, K. Van Tittelboom, S. Steuperaert, P. Dubruel, N. De Belie, Self-healing cementitious materials by the combination of microfibres and superabsorbent polymers, J. Intell. Mater. Syst. Struct. 25 (1) (2014) 13–24.
[10] H.M. Jonkers, A. Thijssen, G. Muyzer, O. Copuroglu, E. Schlangen, Application of bacteria as self-healing agent for the development of sustainable concrete, Ecol. Eng. 36 (2) (2010) 230–235.
[11] J.Y. Wang, H. Soens, W. Verstraete, N. De Belie, Self-healing concrete by use of microencapsulated bacterial spores, Cem. Concr. Res. 56 (2014) 139–152.
[12] C.M. Dry, Three designs for the internal release of sealants, adhesives, and waterproofing chemicals into concrete to reduce permeability, Cem. Concr. Res. 30 (12) (2000) 1969–1977.
[13] K. Van Tittelboom, N. De Belie, D. Van Loo, P. Jacobs, Self-healing efficiency of cementitious materials containing tubular capsules filled with healing agent, Cem. Concr. Compos. 33 (4) (2011) 497–505.
[14] C. Dry, Design of self-growing, self-sensing, and self-repairing materials for engineering applications, in: A.R. Wilson, H. Asanuma (Eds.), Smart Materials Conference, 2001, pp. 23–29.
[15] S. Pareek, A. Oohira, A fundamental study on regain of flexural strength of mortars by using a self-repair network system, in: 3rd International Conference on Self Healing Materials, Bath, UK, 2011, pp. 46–47.
[16] B. Masschaele, V. Cnudde, M. Dierick, P. Jacobs, L. Van Hoorebeke, J. Vlassenbroeck, UGCT: new X-ray radiography and tomography facility, Nucl. Instrum. Methods Phys. Res. Sect. A 580 (1) (2007) 266–269.
[17] B. Masschaele, M. Dierick, D. Van Loo, M. Boone, L. Brabant, E. Pauwels, V. Cnudde, L. Van Hoorebeke, HECTOR: a 240 kV micro-CT setup optimized for research, J. Phys. Conf. Ser. 463 (2013).
[18] J. Vlassenbroeck, M. Dierick, B. Masschaele, V. Cnudde, L. Van Hoorebeke, P. Jacobs, Software tools for quantification of X-ray microtomography at the UGCT, Nucl. Instr. Meth. Phys. Res. Sect. A 580 (1) (2007) 442–445.
[19] Y. Yao, Y. Zhu, Y. Yang, Incorporation of SAP particles as controlling pre-existing flaws to improve the performance of ECC, Constr. Build. Mater. 28 (1) (2011) 139–145.
[20] K. Van Tittelboom, N. De Belie, F. Lehmann, C. Grosse, Use of acoustic emission analysis to evaluate the self-healing capability of concrete, in: International Symposium on Nondestructive Testing of Materials and Structures – NDTMS-2011, submitted, Editor, Istanbul, Turkey, 2011.
[21] E. Tsangouri, D.G. Aggelis, K. Van Tittelboom, N. De Belie, D. Van Hemelrijck, Detecting the activation of a self-healing mechanism in concrete by acoustic emission and digital image correlation, Sci. World J. (2013).
[22] L. Brabant, J. Vlassenbroeck, Y. De Witte, V. Cnudde, M. Boone, J. Dewanckele, et al., Three-dimensional analysis of high-resolution X-ray computed tomography data with Morpho+, Microsc. Microanal. 17 (2011) 252–263.